

A Multi-scale Optimization Learning Framework for Diffeomorphic Deformable Registration

Risheng Liu, *Member, IEEE*, Zi Li, Yuxi Zhang, Chenying Zhao, Hao Huang, Zhongxuan Luo, and Xin Fan, *Senior Member, IEEE*

Abstract—Conventional deformable registration methods aim at solving a specifically designed optimization model on image pairs and offer a rigorous theoretical treatment. However, their computational costs are exceptionally high. In contrast, recent learning-based approaches can provide fast deformation estimation. These heuristic network architectures are fully data-driven and thus lack explicitly domain knowledge or geometric constraints, such as topology-preserving, which is indispensable to generate plausible deformations. To integrate the advantages and avoid the limitations of these two categories of approaches, we design a new learning-based framework to optimize a diffeomorphic model via multi-scale propagations. Specifically, we first introduce a generic optimization model to formulate diffeomorphic registration with both velocity and deformation fields. Then we propose a schematic optimization scheme with a nested splitting technique. Finally, a series of learnable architectures are utilized to obtain the final propagative updating in the coarse-to-fine feature spaces. We conduct two groups of image registration experiments on 3D adult and child brain MR volume datasets including image-to-atlas and image-to-image registrations. Extensive results demonstrate that the proposed method achieves state-of-the-art performance with diffeomorphic guarantee and extreme efficiency.

Index Terms—deformable registration, diffeomorphic registration, learning framework, optimization.

I. INTRODUCTION

REGISTRATION plays a critical role in medical image analysis, which transforms different images into one common coordinate system with matched contents by finding the spatial correspondence between images [1]. It is fundamental to many clinical tasks such as image fusion of different modalities, anatomical change diagnosis, motion extraction, and population modeling. Traditional image registration is

formulated as an optimization problem to minimize image mismatching between a target image and a warped source image, subject to transformation constraints. Deformable registration methods compute a dense correspondence between image pairs [2]. Among them, registration upon displacement fields can only capture small deformations enforcing no one-to-one mapping while Diffeomorphic registration has shown as a more elegant paradigm to capture large deformations and offer solid theoretical properties. There are significant structural differences across human brain scans of different subjects and ages, necessitating registration to analyze the structural variations. Diffeomorphism enforces smoothing deformations that preserve geometric structures. Therefore, the diffeomorphic registration is so general and essential in medical analysis covering not only intra-subject imaging but also population-based and/or longitudinal studies especially when large deformations occur [3]–[5].

Conventional deformable registration techniques aim at solving the optimization problem and offer rigorous theoretical treatments. However, iteratively optimizing which involves gradient computations over high dimensional parameter space and image space makes them computationally intensive and time-consuming [3]–[7]. Recent learning-based methods replace the costly numerical optimization for image pairs with one step of prediction by learned deep networks so that they can provide fast deformation estimation. Balakrishnan *et al.* propose the VoxelMorph, a UNet network structure, to address the deformable image registration [8]. These learning-based approaches lack explicit constraints on the field regularity and other desirable geometric properties. Therefore, their final estimate has no interpretable and theoretical guarantee to physically plausible fields. Recently, the works of [9] combines the VoxelMorph model with the diffeomorphic constraint for topology-preserving deformations. However, these approaches directly establish mappings from volume data to transformations, treating deep learning as a black box.

To address the limitations of both optimization-based and learning-based approaches, we design a new deep propagation framework to optimize a diffeomorphic model via multi-scale propagation for deformable registration. First, we introduce a generic optimization model to formulate the diffeomorphic deformation problem. Rather than performing the optimization over the image domain, we learn a more discriminative feature space enabling us to handle deformations more powerfully. Then we leverage the nested splitting technique to build a schematic optimization that employs deep networks to solve and propagate deformation fields on the learned multi-scale

This work was supported in part by the National Natural Science Foundation of China (NSFC) under Grant Nos. 61922019, 61733002, 61672125 and 61772105, the LiaoNing Revitalization Talents Program (XLYC1807088) and the Fundamental Research Funds for the Central Universities. (*Corresponding author: Xin Fan*).

R. Liu, Z. Li, Y. Zhang, Z. Luo and X. Fan are with the DUT-RU International School of Information Science and Technology, Dalian University of Technology, Dalian, 116620, China, and also with the DUT-RU Health Care Intelligent Computing Joint Research Center (e-mail: rslu@dlut.edu.cn; alisonbrielee@gmail.com; yuxizhang@mail.dlut.edu.cn; zxlue@dlut.edu.cn; xin.fan@ieee.org).

C. Zhao and H. Huang are with the Department of Radiology, Children’s Hospital of Philadelphia, Philadelphia, PA, United States. C. Zhao is also with the Department of Bioengineering, School of Engineering and Applied Science, University of Pennsylvania, Philadelphia, PA, United States. H. Huang is also with the Department of Radiology, Perelman School of Medicine, University of Pennsylvania, Philadelphia, PA, United States (e-mail: chenyzh@seas.upenn.edu; huangh6@email.chop.edu).

Z. Luo is also with the Institute of Artificial Intelligence, Guilin University of Electronic Technology, Guilin, China.

feature space. This optimization perspective differentiates our scheme from naively cascading Convolutional Neural Networks (CNNs) in most existing learning-based approaches, leading to the computational interpretation of network architectures that guarantees diffeomorphism.

This work bridges deep learning with optimizing a diffeomorphism model for medical image registration while applicable to other registration scenarios requiring geometric constraints. The main contributions of this work can be summarized in the following aspects:

- We establish a diffeomorphic deformable model with both velocity and deformation fields on the feature space and develop a schematic multi-scale optimization scheme using the nested splitting technique. We then establish a general multi-scale optimization learning framework with geometric constraints, propagating learned multi-scale features and deep parameters.
- We build key deep modules to incorporate domain knowledge, latent data distribution, and geometric constraints in our end-to-end optimization learning framework, during the multi-scale propagating process. Our nested splitting optimization technique yields these interpretable deep modules for our multi-scale optimization learning framework and inspires training losses adaptive to scales.
- We provide an optimization perspective for learning based registration rather than simply cascading CNN modules, able to interpret our learning-based registration as the optimization of energy with explicit geometric constraints. Moreover, the proposed optimization learning framework circumvents the time-consuming computations of iterative gradients for conventional approaches, rendering high-speed optimization.

Extensive evaluations on both image-to-atlas and the image-to-image registration tasks for 3D adult and child brain MRI demonstrate that our approach achieves state-of-the-art performance with the diffeomorphic guarantee and extreme efficiency over both existing optimization-based and learning-based approaches.

II. RELATED WORK

Conventional registration methods [5] [10] [11] [4] solve an optimization over the transformations. Common representations are displacement vector fields, such as the b-splines model with control points [12] [7], elastic-type models [13]. Some algorithms perform TV-regularized image registration [10] [11]. To avoid implausible registration fields, large displacement fields are strongly penalized. Therefore, these approaches have difficulties capture large deformations. To capture large deformations and guarantee mathematical properties, such as topology-preserving, diffeomorphic registration [3]–[6] [14]–[16] has been extensively developed. Diffeomorphic frameworks use smooth flow fields to represent the deformation, the regularization is typically introduced as part of the ordinary differential equation constraining on the vector fields. However, classical diffeomorphic deformation methods have very large numbers of parameters, too time-assuming and complicated to work with.

Recently, learning-based methods [17]–[19] [8], taking advantage of CNNs have shown impressive results, especially in terms of runtime. Supervised methods [17]–[19] have widely applied in registration. But ground truth registration fields are hard and expensive to obtain, which are often derived via conventional registration tools. It can be circumvented by the unsupervised methods. Inspired by the VoxelMorph [8] [9], research [20]–[23] has focused on replacing costly numerical optimization with global function optimization over the training data in an unsupervised way. However, most existing learning-based approaches leverage a deep architecture for generic tasks, *e.g.*, UNet, with a designated loss for registration, establishing mappings from volume data to transformations. They only employ regularization implicitly determined by cost function, also offer limited registration fields regularity. Moreover, they do not necessarily provide one-to-one mapping and preserve topology.

The work of Marc et al. [24] learns a spatially-varying regularizer within a registration model. They leave integration with predictive registration approaches for future work. Some works [9] [20] propose to estimate the velocity fields or momentum fields, which can be used to obtain diffeomorphic transformations. Similar to our method, the diffeomorphic variant of the VoxelMorph model [9] also makes use of CNNs to learn the diffeomorphic transformation. However, they directly estimate the velocity field without employing constraints on it. In this paper, we propose a new learning-based optimization framework for energy-based model [25] of diffeomorphic registration. Inspired by the optimization-based model, we parameterize our registration model by priors-inspired deep architectures, leading to networks with explicit geometric constraints. We build three key learning modules that approximate the optimization steps of an energy with explicit diffeomorphic constraint. Besides, we perform the registration on the multi-scale feature space, which makes our method extremely efficient.

III. METHOD

In this section, we first introduce a generic optimization model to formulate diffeomorphic deformable registration with both velocity and deformation fields on feature space. Then we propose a multi-scale schematic optimization scheme based on the nested splitting techniques. In the next section, we present our multi-scale neural network framework to obtain the final deformation field in a coarse-to-fine way.

A. Diffeomorphic Deformable Model on Feature Space

To capture large deformations, diffeomorphic registrations are frequently employed. These fluid-based methods [3] [5] [24] [17] have many desirable mathematical properties, such as invertibility, globally one-to-one smooth, and topology-preserving. The final deformation field is obtained via integrating a series of time-dependent vector fields over time. In this work, we introduce a generic optimization model to formulate diffeomorphic deformable registration with both velocity and deformation fields. Given a source image \mathbf{I}_s and a target image \mathbf{I}_t with a spatial domain $\Omega \in \mathbb{R}^d$, specifically,

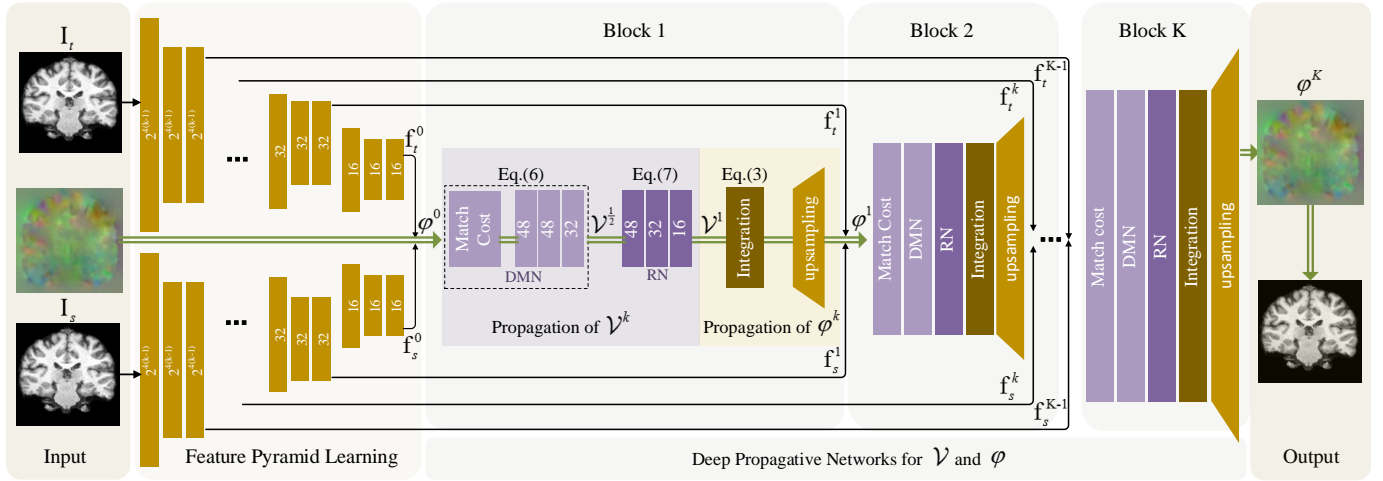


Fig. 1. Our pipeline optimizes a diffeomorphic deformation model by propagating learned deep networks in a coarse-to-fine way. Each iterative block at one scale sequentially propagates the optimizations for registration fields. The velocity and deformation fields, \mathcal{V} and ϕ are updated in an alternative and collaborative manner. We cascade a feature-based data match module and a geometric regularization module to propagate the optimization for \mathcal{V} in Eq. (6) and Eq. (7) while assembling integration and upsampling for the propagation of ϕ in Eq. (3). The double lines indicate the direction of the registration field propagation. The single line indicates the flow of features.

we aim at minimizing the following constrained optimization model:

$$\begin{aligned} & \min_{\varphi, \mathcal{V}} E_D(\mathcal{V}, \varphi; \mathbf{f}_s, \mathbf{f}_t) + E_R(\mathcal{V}), \\ & s.t. \frac{\partial \phi(t)}{\partial t} = \mathcal{V}(\phi(t)), \phi(0) = Id, \varphi = \phi(1), \end{aligned} \quad (1)$$

where $\varphi : \Omega \times \mathbb{R} \rightarrow \Omega$ is the final deformation field, \mathcal{V} is the velocity fields for unit time, $\phi(0) = Id$ is the identity transformation, $t \in [0, 1]$ represents the time, such that the final registration field φ is obtained via integration of a series of velocity fields \mathcal{V} over time t . And we perform registration on feature space, $\mathbf{f}_s, \mathbf{f}_t$ is the feature representations of the source and target images. E_D is a data matching term, involving the velocity field \mathcal{V} and the final deformation field φ , forcing the image similarity. E_R is a regularization term that guarantees the smoothness of the registration fields, constraining on the velocity fields \mathcal{V} . Different from conventional diffeomorphic registrations methods, such as Large Displacement Diffeomorphic Metric Mapping (LDDMM) models [5] [24] [17] [20], which solve the optimization on the image domain, we propose to jointly optimize velocity and deformation fields on the multi-scale feature space.

B. Multi-scale Schematic Optimization Scheme

In this section, we develop a multi-scale schematic optimization scheme to generate the propagation sequence (denoted as $\{\mathcal{V}^k, \varphi^k\}$ where k means different scales and $k = K$ describes the original scale) based on the constrained optimization model in Eq. (1). We design the cascaded propagations of the \mathcal{V}^k and φ^k as:

$$\begin{cases} \mathcal{V}^{k+1} = \arg \min_{\mathcal{V}} E_D(\mathcal{V}, \varphi^k; \mathbf{f}_s^k, \mathbf{f}_t^k) + E_R(\mathcal{V}), & (2) \\ \varphi^{k+1} = \phi(1) \text{ with } \frac{\partial \phi(t)}{\partial t} = \mathcal{V}^{k+1}(\phi(t)), \phi(0) = Id, & (3) \end{cases}$$

where the update of \mathcal{V} dependent on the previous φ^k and the features, each deformation field φ^k is obtained via the integration of current \mathcal{V} , governed by the ordinary differential equation $\phi(t) = \mathcal{V}(\phi(t), t)$. The deformation and velocity fields are updated in an alternative and collaborative manner.

For each \mathcal{V}^{k+1} , rather than directly calculating from \mathcal{V}^k , as shown in Eq. (2), we design a two-step update, corresponding to the data match term and regularization term, respectively, as:

$$\begin{cases} \mathcal{V}^{k+\frac{1}{2}} = \arg \min_{\mathcal{V}} E_D(\mathcal{V}, \varphi^k; \mathbf{f}_s^k, \mathbf{f}_t^k), & (4) \\ \mathcal{V}^{k+1} = \arg \min_{\mathcal{V}} \frac{1}{2} \|\mathcal{V} - \mathcal{V}^{k+\frac{1}{2}}\|^2 + E_R(\mathcal{V}), & (5) \end{cases}$$

then we propose efficient deep architectures to complete the above propagation. In the next section, we show how to employ deep networks to update the subsequence of \mathcal{V}, φ .

C. Multi-scale Neural Network Framework

To begin with, our method transforms image pairs from the image domain to the feature space. Then we design deep propagative architectures to solve the diffeomorphic deformable model on the feature space with the multi-scale optimization scheme in section B. Specifically, we first use the feature extraction network to produce two sets of feature maps with different spatial resolutions. Then, We build deep propagative modules, data matching, regularization, and integration to approximate optimization steps in Eqs. (3), (4) and (5). Next, we will explain the main ideas for each part.

1) *Feature Pyramid Learning*: Given an image pair, we employ three-layers CNN to extract two pyramids of feature representations of the source and target images at each scale {denoted as $\mathbf{f}_s^k, \mathbf{f}_t^k$ }. At each block, we downsample the features at the previous block by a factor of 2. These feature pyramids are prepared for establishing accurate spatial correspondence later. Computing at full resolution can

easily exhaust the memory, while performing on the more discriminative multi-scale feature space not only reduces the computational cost but also makes our method more powerful.

2) *Deep Propagative Architectures*: Given an image pair, we employ three-layers CNN to extract two pyramids of feature representations of the source and target images at each scale $\{\text{denoted as } \mathbf{f}_s^k, \mathbf{f}_t^k\}$. Then, we use two residual type deep CNNs to propagate \mathcal{V}^k and $\mathcal{V}^{k+\frac{1}{2}}$. We apply the Data Match Network (DMN) and the Regularization Network (RN) followed by Integration for the subsequence updating, respectively. Note that, we jointly optimize the data matching cost and the regularizer, corresponding to the data match module and the regularization module, respectively.

Data matching module. We resemble evolving energy gradients in Eq. (4) by cascading DMN. To establish accurate voxel-to-voxel correspondence and reduce the feature space distance between image pairs, we extra introduce a matching cost $M(\mathbf{f}_s^k, \mathbf{f}_t^k, \varphi^k)$, which measures the misalignment of the corresponding voxels of the two feature maps. We process it using a three-layer CNN to propagate the $\mathcal{V}^{k+\frac{1}{2}}$. We interpret the data matching network as:

$$\mathcal{V}^{k+\frac{1}{2}} = \mathcal{N}_D(\mathcal{V}^k, M(\mathbf{f}_s^k, \mathbf{f}_t^k, \varphi^k); \mathcal{W}_D^k), \quad (6)$$

where $M(\mathbf{f}_s^k, \mathbf{f}_t^k, \varphi^k) = |\mathbf{f}_t^k - \mathbf{f}_s^k \circ \varphi^k|$, \mathcal{W}_D^k are the learnable parameters of the data matching network at each scale. To construct the matching cost, we perform feature warping, transforming the features of the source image using the deformation field from the previous block at each block. Specifically, we use the spatial transform function [8] [26] to perform this warp operation. The feature-space distance between image pairs is reduced at each DMN and this process is repeated until the output scale. The DMNs at different scale share the same network structure but have their parameters.

Regularization module. Minimizing the data match term corresponds to the idea of finding the deformation field yielding the smallest mismatch. Since this process tends to be unstable due to ambiguity, the deformation field that is merely computed by the data match term is fragile to outliers. To tackle this problem, we introduce our regularization strategy, corresponding to the Eq. (5). We employ a data-driven regularization network with designated loss functions to produce smooth enough velocity fields. We propose to use contextual information to post-process the velocity field. Its design is based on dilated convolutions, which effectively enlarges the receptive field size of each output unit. We apply a three-layer network to implement propagate \mathcal{V}^{k+1} as:

$$\mathcal{V}^{k+1} = \mathcal{V}^{k+\frac{1}{2}} - \mathcal{N}_R(\mathcal{V}^{k+\frac{1}{2}}; \mathcal{W}_R^k), \quad (7)$$

where \mathcal{W}_R^k are the learnable parameters of refinement network at the k -th block. It takes the velocity fields from the data matching network and outputs refined velocity fields.

Integration module. At each block, the deformation field is defined through the ordinary differential equation in Eq. (3). We compute the integration using the efficient scaling and squaring [3] [4] [8] method. It is an approximation to continuous integration. We use the Euler method to solve the ordinary differential equation in Eq. (3). Specifically, it recursively computes the solution at successive small time-steps h

TABLE I
ABLATION EXPERIMENTS ON MODEL CONFIGURATIONS.

Model	Test		PPMI	
	Dice	LNCC	Dice	LNCC
Full model	0.770	0.247	0.781	0.243
RN (1 layer)	0.763	0.234	0.777	0.229
DMN (1 layer)	0.741	0.199	0.757	0.196
RN (6 layers)	0.771	0.239	0.784	0.236
DMN (6 layers)	0.777	0.249	0.788	0.245

as: $\phi(t+h) = \phi(t) + h\mathcal{V}(\phi(t)) = (x+h\mathcal{V}) \circ \phi(t)$, where the small field at a single step can be regarded as an Euler integration. For example, the solution with eight steps are given as: $\phi(1/8) = x + \mathcal{V}(x)/8$, $\phi(1/4) = \phi(1/8) \circ \phi(1/8)$, $\phi(1/2) = \phi(1/4) \circ \phi(1/4)$, $\phi(1) = \phi(1/2) \circ \phi(1/2)$.

D. Loss function

We use the multi-scale training loss proposed in FlowNet [18] [19]. The complete similarity loss is the sum of the training loss at each scale. The training loss consists of image similarity loss and smoothness loss. For a 4-scale model, from the zeroth to the third scale, the weights for each pyramid loss are set to $\{0.02, 0.08, 0.32, 10\}$, with the last scale corresponding to the input images.

1) *Similarity loss on deformation fields*: We use the Local Normalized Cross Correlation as image similarity loss, which is a point-wise measure metric, designed for image registration tasks. It is computed by averaging Normalized Cross Correlation scores of overlapping sliding windows centered at sampled voxels. Note that, when computing similarity loss, we scale the image pairs and warp the downsampled images with the deformation fields at different scales. At each scale, we use different window sizes to compute the local normalized correlation coefficient. We use a smaller window size for the lower resolution. From the zeroth to the third scale, the window sizes are set to $\{3, 5, 7, 9\}$, respectively.

2) *Smoothness loss on velocity fields*: We employ a smoothness loss at each scale. We define it as the diffusion regularizer on spatial gradients of the velocity fields. The trade-off weight between regularization loss and similarity loss is set to be 15.

E. Implementation

We then introduce our detailed configurations. We use filters of the size $3 \times 3 \times 3$ for all the convolutional layers. All convolutional layers are followed by a leaky ReLU function except the one that outputs the registration field. Computation on the full resolution may easily exhaust the memory, thus we compute at low resolution. In our multi-scale model, we choose to output a half-resolution smooth enough deformation field and up-sample it via interpolation [8] [26] to obtain the full-resolution deformation field.

IV. EXPERIMENTAL RESULTS

This section first explores the impact of each part of our paradigm. Next, we compare our algorithm with the state-of-the-art deformable registration techniques to demonstrate its superiority on accuracy, efficiency as well as diffeomorphism preservation of the deformation.

TABLE II
ABLATION ANALYSIS ON BLOCK COMPONENTS AND NUMBERS.

-		1-block		2-block		3-block	
DMN		✓	✓	✓	✓	✓	✓
RN		✗	✓	✗	✓	✗	✓
Test	Dice	0.738 (0.028)	0.745 (0.024)	0.767 (0.017)	0.770 (0.015)	0.769 (0.015)	0.770 (0.016)
	LNCC	0.226 (0.005)	0.225 (0.005)	0.238 (0.004)	0.247 (0.004)	0.235 (0.005)	0.244 (0.004)
PPMI	Dice	0.758 (0.018)	0.762 (0.016)	0.779 (0.013)	0.781 (0.012)	0.780 (0.012)	0.782 (0.012)
	LNCC	0.224 (0.004)	0.222 (0.004)	0.234 (0.004)	0.243 (0.004)	0.231 (0.004)	0.241 (0.004)

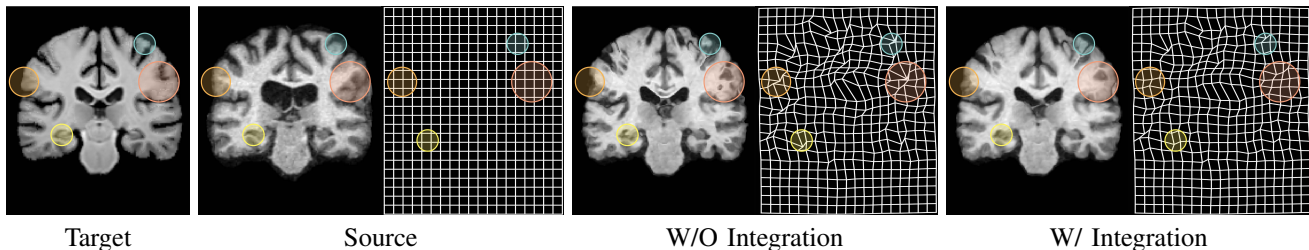


Fig. 2. Comparisons on deformation grids by warping the moving to the target without and with the integration module. Singularities emerge in the circled fields when applying no integration.

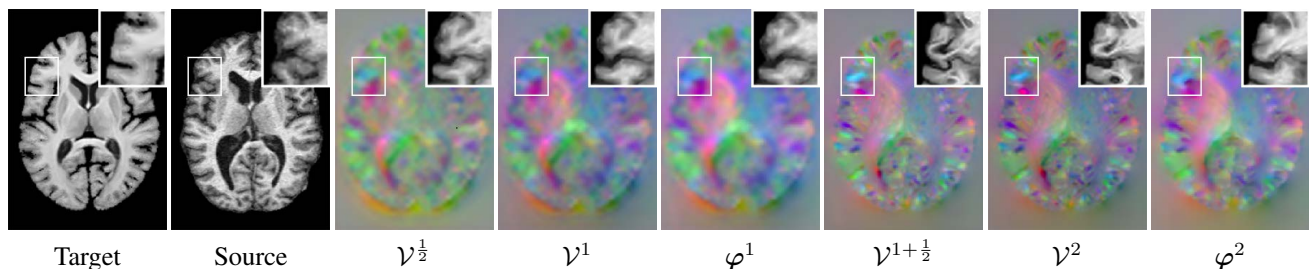


Fig. 3. The evolution of deformation color maps and registered images with the propagation of \mathcal{V} and ϕ in the first two blocks.

A. Data Preparation and Training

We evaluate different imagesets. The first dataset, called multi-site data, includes 427 T1 weighted MR volumes from three publicly available datasets: ADNI [27], ABIDE [28], PPMI [29] and OASIS [30]. The second dataset, called child data, consists of T1-weighted 12 child brain scans from HCP [31]. Considering the large disparity among different datasets, all scans were preprocessed with motion correction, NU intensity correction, normalization, skull stripping, and affine registration. Experimentally, we use FreeSurfer [32] software to perform skull stripping and use FSL [33] software for affine registration.

In the multi-site dataset, Evaluations are conducted in two different sights, one aligning all the source data to a common atlas called image-to-atlas registration, and the other addressing general registration between two arbitrary volumes called image-to-image registration. For both of these two cases, the multi-site dataset except PPMI is split into 281, 17, and 70 for training, validation, and testing, respectively. The unseen PPMI [29] dataset containing 59 scans is also employed for testing. Specifically, for the image-to-atlas registration, we use the publicly available atlas form [8] as the target, and for image-to-image case, the target images are randomly selected from datasets. These experiments enable not only assessment of performance on a large dataset but also the evaluation of scans that were not observed by the deep networks during

training. In the second dataset, we fine-tune the model already trained in the first dataset on adult scans, and then use it to perform image-to-atlas registration on those 12 child scans. This experiment enables us to assess the ability of our algorithm to register on a different scenario (child brain data).

The proposed propagation network is jointly trained in an unsupervised end-to-end way with TensorFlow [34] package on an device of NVIDIA TITAN XP. It takes about 14 hours to train our model from scratch in 28100 iterations. During training, we use Adam optimizer [35] with a learning rate of $1e^{-4}$. To reduce memory usage, the images are cropped to $160 \times 192 \times 224$ and the batch size is set as 1.

B. Evaluation Metrics

To achieve a more comprehensive evaluation, both the average Dice score [36] over registered testing pairs and the Jacobian matrix over the computed deformation are considered as evaluation metrics, to evaluate the anatomical overlap correspondences of the registered volume pairs and the smoothness of the deformation fields, respectively.

To calculate the Dice score, segmentation is performed with FreeSurfer on each of the testing volume to extract 30 anatomical structures, on which the average Dice is calculated. The Jacobian matrix $\mathbf{J}_\phi(\mathbf{x}) = \nabla\phi(\mathbf{x})$ captures the local properties of ϕ around voxel \mathbf{x} , such as stretching and rotating. The Jacobian of a deformation that conforms to be a flow field is always

TABLE III

THE FIRST THREE ROWS GIVE THE DICE OF DIFFERENT METHODS FOR IMAGE-TO-ATLAS [1], IMAGE-TO-IMAGE [2] REGISTRATION ON MULTI-SITE DATASET AND REGISTRATION RESULTS [3] ON THE CHILD DATASET. STANDARD DEVIATIONS ARE IN BRACKET. THE MIDDLE THREE ROWS INDICATE THE FOLDS THAT OCCURRED IN DEFORMATION FIELDS WITH THE PERCENTAGES PARENTHEZIZED. THE LAST ROW LISTS THE EXECUTION TIME.

Method	RCN	Elastix	NiftyReg	VM	ANTs-V1	ANTs-V2	Ours
Dice [1]	0.436 (0.017)	0.715 (0.032)	0.753 (0.026)	0.768 (0.018)	0.749 (0.136)	0.768 (0.020)	0.778 (0.015)
Dice [2]	0.400 (0.023)	0.724 (0.034)	0.773 (0.026)	0.757 (0.035)	0.781 (0.039)	0.777 (0.030)	0.783 (0.023)
Dice [3]	0.472 (0.017)	0.729 (0.017)	0.773 (0.012)	0.768 (0.013)	0.767 (0.016)	0.677 (0.030)	0.776 (0.010)
Folds [1]	0	91 (0.001)	393 (0.005)	40674 (0.591)	9662 (0.140)	0	0
Folds [2]	0	642.2 (0.009)	39699 (0.576)	52798 (0.767)	39443 (0.573)	0	0
Folds [3]	0	0	9576 (0.139)	30716 (0.44)	28379 (0.412)	0	0
Time (s)	0.558 (0.017)	83 (10)	435 (39)	0.558 (0.017)	1888 (129)	4614 (1030)	0.384 (0.010)

positive. Its determinant suggests the relative volumes before and after transformation, so negative determinants mean the loss of the one-to-one mapping [4]. So the local deformation is diffeomorphic at the locations where $|\mathbf{x} : \mathbf{J}_\phi(\mathbf{x})| > 0$. We count all the folds, where $(|\mathbf{x} : \mathbf{J}_\phi(\mathbf{x})| \leq 0)$, and use Folds to represent the number of folds.

C. Ablation Analysis

We investigate the role of different propagation components in our model, including the regularization module, multi-scale degree as well as the architecture of the data match network and regularization network. Experiments are conducted on the testing data of the mixed datasets (referred as Test) and the unseen PPMI dataset (referred as PPMI), in the case of image-to-atlas registration. Except for the Dice score, we also provide the Local Normalized Correlation Coefficient (LNCC) as evaluation metric.

First, we consider the case where the regularization network is eliminated and only the data match network is engaged for three-block process, to figure out the significance of smoothness regularization on the deformation field. From Tab. II we can see that the participation of smoothness regularization can ideally exploit the context information to refine the predicted field and obviously promote the registration performance. In addition, we can see that a deeper network architecture could more easily get stuck at overfitting, which can be solved by employing more training data. We adopt the 2-block model to perform the following experiments as our method.

Further, we compare the effect of network architecture by changing the number of convolutional layers of either data match network or regularization network and keeping the rest the same. Tab. I shows that the larger-capacity data match network leads to better results, resembling the critical role of data matching term for the accurate spatial correspondence.

Except for the propagation networks, the advantage of numerical integration on velocity field is also explored. Fig. 2 illustrates the warped images and the corresponding flow grids generated by model with and without integration operation. Apparently, the integration on velocity can properly reduce unreasonable overlaps of deformation field and preserve the topology of the warped volume, promising a smoother and more reliable registration.

To provide an intuitive comprehension on the effect of each component, Fig. 3 visualizes the deformation fields generated in each step during the multi-stage process, and

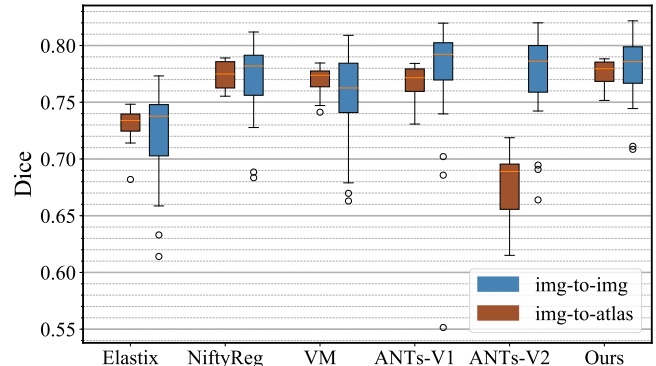


Fig. 4. Box-plots of Dice scores obtained by different registration methods.

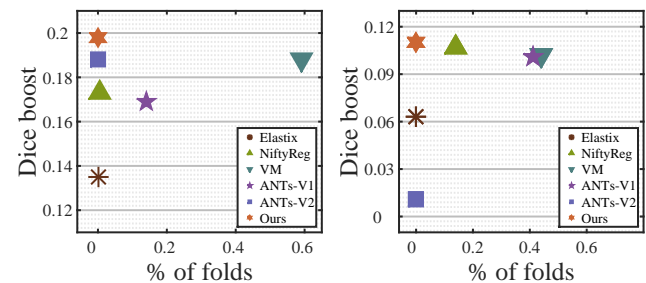


Fig. 5. The plots of Dice boost VS percentage of folds. Dice boost represents the Dice value increase from simple affine registration. The left and right demonstrate the image-to-atlas registration results on adult and child dataset, respectively. The top-left corner indicates the desired performance.

the enlargement of corresponding local detail is attached on the bottom right. As the visualization shows, the data match network firstly provides a primary estimation of field $\mathcal{V}^{\frac{1}{2}}$, whereafter the regularization network refines the field to make \mathcal{V}^1 smoother. Further, the integration operation ideally reduces the unreasonable overlaps within the field and guarantees a diffeomorphic deformation ϕ^1 . Repeating this way, the propagated field can be guided towards the desirable results and achieves satisfying registration accuracy.

D. Comparisons with Existing Methods

We compare our approach with five state-of-the-art registration techniques, including three widely-used optimization-based public registration tools: Elastix [37], Symmetric Normalization (SyN) [38] and NiftyReg [7], and two latest learning-based methods: VoxelMorph [8] and Recursive Cascaded Networks [22], referred as VM and RCN.

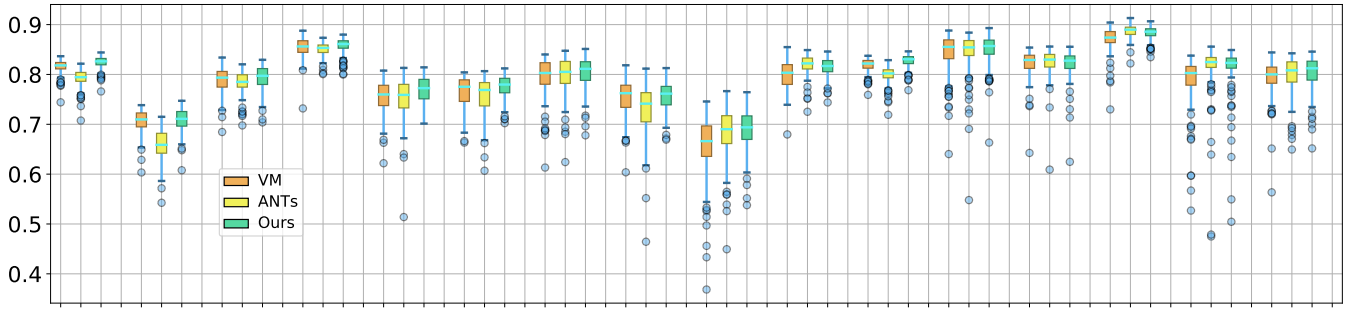


Fig. 6. Boxplots show the Dice scores for ANTs-V2, VM and our method over sixteen anatomical structures including Cerebral White Matter (CblmWM), Cerebral Cortex (CblmC), Lateral Ventricle (LV), Inferior Lateral Ventricle (ILV), Cerebellum White Matter (CerebWM), Cerebellum Cortex (CerebC), Thalamus (Tha), Caudate (Cau), Putamen (Pu), Pallidum (Pa), Hippocampus (Hi), Accumbens area (Am), Vessel, Third Ventricle (3V), Fourth Ventricle (4V), and Brain Stem (BS).

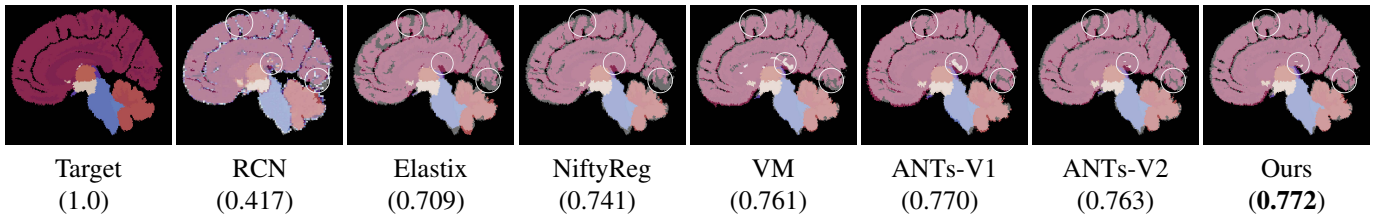


Fig. 7. Registered MR slices overlaid with atlas using different methods. The Dice scores are given in the bottom parentheses. Circles indicate several evident inconsistencies.

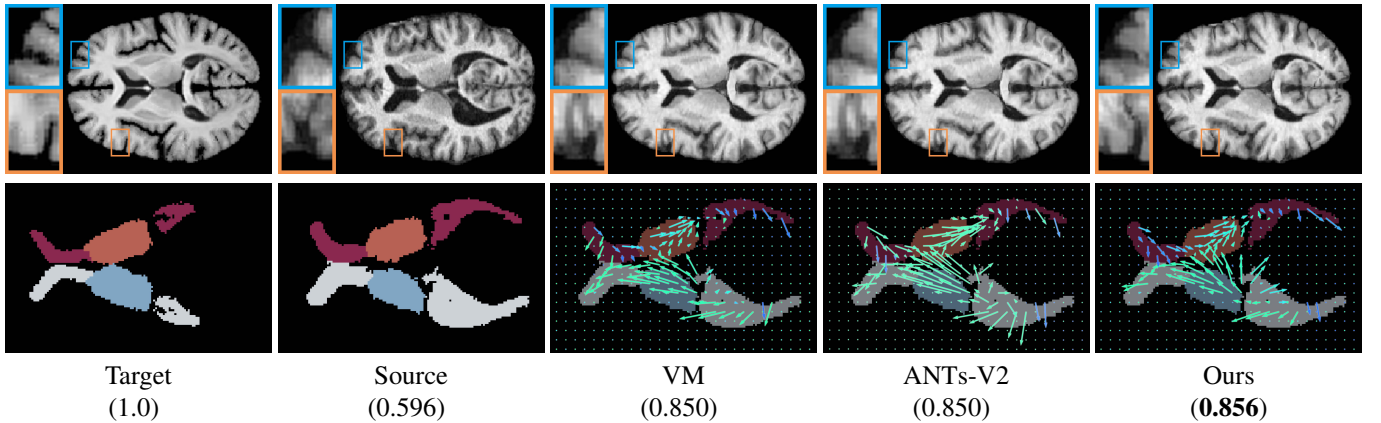


Fig. 8. Registered results of segmented anatomical structures using VM, ANTs-V2 and our method with the Dice scores parenthesized.

The parameter settings of the conventional methods are as follows. For Elastix, we run B-spline registration with Mattes Mutual Information as a similarity metric. Four scales are used with 500 iterations per scale and the control point spacing of the b-spline transformation is set to 16 voxels. For the SyN algorithm implemented in the ANTs [39] package, we take Cross Correlation (CC) as the similarity measure metric. We use the SyN step size of 0.25, Gaussian parameters (9, 0.2), at three scales with at most 201 iterations each. In addition, we also use the SyN step size of 0.1 as a second baseline with 4 scales to perform more iterations, which results in longer runtime and better performance (referred to as ANTs-V1 and ANTs-V2, respectively). As for NiftyReg, we use the Normalized Mutual Information as the similarity measure. We run it with the multi-threaded CPU version of 12 threads using 1500 iterations. As for the learning-based approaches,

we fine-tune these models on our training datasets for fairness. We run Elastix, ANTs, and NiftyReg on a PC with i7-8700 (@3.20GHz, 32G RAM), while learning-based methods on NVIDIA TITAN XP.

First, we quantitatively evaluate the accuracy, rationality and time consumption of all these techniques for both cases of image-to-atlas and image-to-image registration, in terms of Dice score, fold number, and runtime. Tab. III demonstrates that our method outperforms all comparison methods in accuracy and diffeomorphism, including the top-performing conventional registration techniques. Our method outputs accurate (dice values) deformation fields with zero folds, preserving the diffeomorphism, comparable to optimization-based ANTs-V1 and ANTs-V2, meanwhile runs significantly faster than these two. Among learning-based methods, we takes the least time, exceeding the most efficient learning framework VoxelMorph

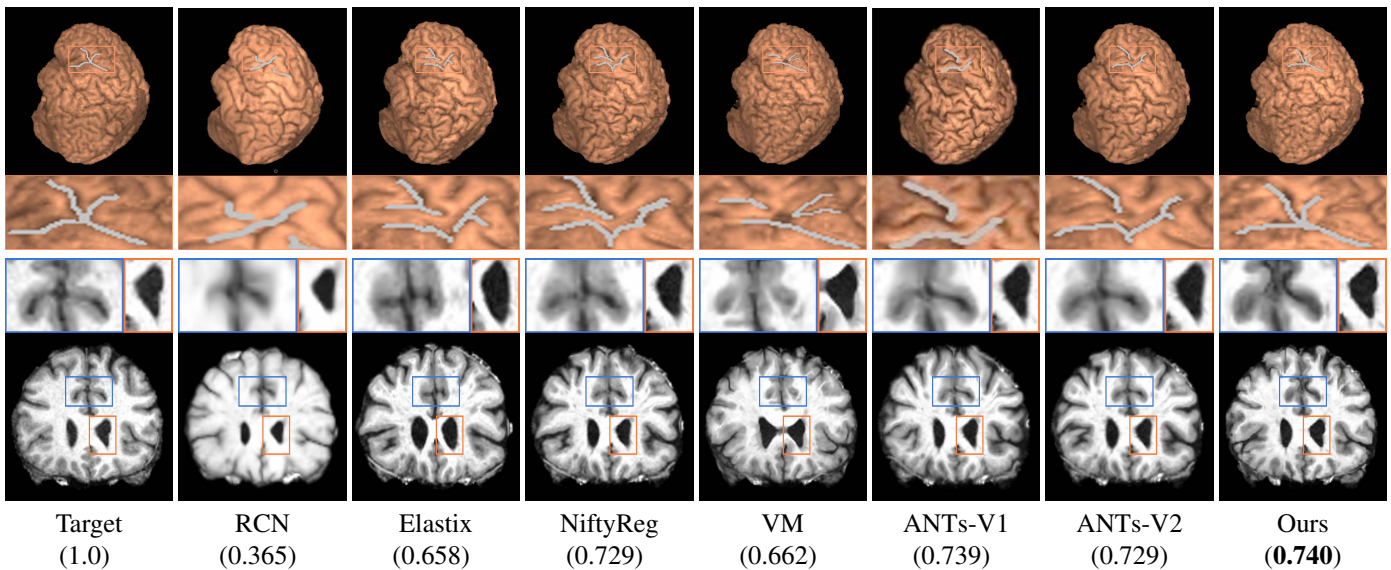


Fig. 9. The first two rows demonstrate cortex visualization and zoomed-in overlaid sulci registered using different methods. The last two rows give the MR slices and zoomed-in warped patches for image-to-image registration. The higher coincidence with the target indicates the better registration. Parenthesized values in the bottom give Dice scores.

(0.384s and 0.558s), over 30% less than it. In addition, ours gives higher Dice score in less running time, benefiting of the well-designed network architectures, and dealing with half-resolution rather than the original scale further accelerates the estimation process.

Fig. 4 depicts the stability of the methods in view of box-plot of Dice score, where less outliers and lower variance indicate a more stable registration. As we can see the optimization-based methods perform slightly better for the image-to-image registration where the image pairs are much more similar with each other, but less satisfying for the other case. While our method gives a obvious lower variance with a comparable mean of Dice for both these two case, showing stronger stability. Fig. 5 represents the comprehensive comparison of Dice boost and folds, the orange marker on the top left showing a higher consistence between the registered pairs and a lower discrepancy of the deformation field.

To take a deeper perspective of alignment of anatomical segmentation. We illustrate the Dice score of 30 anatomical structures in Fig. 6. Limited by space, besides our method, we only present ANTs-V2 and VM as the representatives for the optimization-base and learning-base techniques. We can see that compared with the conventional method ANTs-V2, the deep method VM gives evenly accuracy but performs much less stable among different anatomical segmentations. While our deep model achieves a good balance between the accuracy and stability in virtue of a proper trade-off between the model-based domain knowledge and data-based deep representation. Fig. 7 visualizes one slice of the registered segmentations with Dice score generated by different methods. The target is set as semitransparent on the upper layer to present an intuitive discrepancy between the results and target. We can see that our method has higher consistence with the target for both interior and outline.

Except for the boost of accuracy, we can also ideally

promote efficiency in virtue of the well-designed network and ably-nested regularization on estimated flow, such as context information and integration operation. Fig. 8 visualizes both the direction and magnitude of the generated flow with less than one percent of folds for about 5 million voxels within a brain volume (the upper row) and the corresponding 2D slice with a blowup of details on the right (the lower row). As the pictures on the below row show, the flow generated by our method contains fewer displacements, indicating a simpler transformation, which is confirmed experimentally, the runtime of VM, ANTs-V2 (MI) and ours are 0.58s, 1330s, and 0.42s, respectively. Accordingly, the magnified details on the lower pictures demonstrate qualitatively the superiority of our method over the competitors.

Fig. 9 depicts the 3D view of cortical modeling and 2D slices of the registration results, from which we can see that our method can ideally guarantee the topology of the registered volumes and preserve the contour of anatomical structure like cerebral cortex and ventricles.

V. CONCLUSION

We introduce a generic optimization model to formulate diffeomorphic registration with both velocity and deformation fields. The framework propagates learned multi-scale features and deep parameters for optimization, and thus renders fast optimization without needing iteratively computing gradients on the image domain. On the other hand, we design the learned propagating networks upon the nested splitting technique for optimization so that the deep propagation is able to guarantee the diffeomorphic constraint for accurate registration without folds. We conduct two groups of image registration experiments on 3D adult and child brain MRI datasets including image-to-atlas and image-to-image registrations. Extensive results show that our method achieves state-of-the-art performance with diffeomorphic guarantee and extreme

efficiency. We demonstrate the performance on MRI images, and future validation remains on cross-modal registration and other scenarios where the moving and target exhibit significant appearance differences.

It is not desirable to simply bring deep architectures or optimization techniques for generic registration to medical studies because medical registration requires preserving anatomical structures especially when large deformations occur. In this paper, we address the challenging issue to efficiently solve optimization energy with diffeomorphism that preserves geometrical structures. Our approach is applicable to other computer vision tasks, *e.g.*, panoramic creation, and video super-resolution, where registration with structural preservation is crucial.

SUPPLEMENTAL MATERIALS

This supplementary material provides additional registration examples illustrating our performance further.

REFERENCES

- [1] J. B. A. Maintz and M. A. Viergever, "A survey of medical image registration," *Medical Image Analysis*, vol. 2, no. 1, pp. 1–36, 1998.
- [2] A. Sotiras, C. Davatzikos, and N. Paragios, "Deformable medical image registration: A survey," *IEEE Transactions on Medical Imaging*, vol. 32, no. 7, pp. 1153–1190, 2013.
- [3] V. Arsigny, O. Commowick, X. Pennec, and N. Ayache, "A log-euclidean framework for statistics on diffeomorphisms," in *International Conference on Medical Image Computing and Computer Assisted Intervention*, 2006, pp. 924–931.
- [4] J. Ashburner, "A fast diffeomorphic image registration algorithm," *NeuroImage*, vol. 38, no. 1, pp. 95–113, 2007.
- [5] M. F. Beg, M. I. Miller, A. Trounev, and L. Younes, "Computing large deformation metric mappings via geodesic flows of diffeomorphisms," *International Journal of Computer Vision*, vol. 61, no. 2, pp. 139–157, 2005.
- [6] B. B. Avants, C. L. Epstein, M. Grossman, and J. C. Gee, "Symmetric diffeomorphic image registration with cross-correlation: evaluating automated labeling of elderly and neurodegenerative brain," *Medical Image Analysis*, vol. 12, no. 1, pp. 26–41, 2008.
- [7] W. Sun, W. J. Niessen, and S. Klein, "Free-form deformation using lower-order b-spline for nonrigid image registration," in *International Conference on Medical Image Computing and Computer Assisted Intervention*, 2014, pp. 194–201.
- [8] G. Balakrishnan, A. Zhao, M. R. Sabuncu, J. Guttag, and A. V. Dalca, "Voxelmorph: A learning framework for deformable medical image registration," *IEEE Transactions on Medical Imaging*, vol. 38, no. 8, pp. 1788–1800, 2019.
- [9] A. V. Dalca, G. Balakrishnan, J. Guttag, and M. R. Sabuncu, "Unsupervised learning of probabilistic diffeomorphic registration for images and surfaces," *Medical Image Analysis*, vol. 57, pp. 226–236, 2019.
- [10] V. Vishnevskiy, T. Gass, G. Szekely, C. Tanner, and O. Goksel, "Isotropic total variation regularization of displacements in parametric image registration," *IEEE Transactions on Medical Imaging*, vol. 36, no. 2, pp. 385–395, 2017.
- [11] S. Hermann and R. Werner, "Tv-l1-based 3d medical image registration with the census cost function," in *Pacific-Rim Symposium on Image and Video Technology*, 2013, pp. 149–161.
- [12] D. Rueckert, L. I. Sonoda, C. Hayes, D. L. Hill, M. O. Leach, and D. J. Hawkes, "Nonrigid registration using free-form deformation: Application to breast mr images," *IEEE Transactions on Medical Imaging*, vol. 18, no. 8, pp. 712–721, 1999.
- [13] R. Bajcsy and S. Kovacic, "Multiresolution elastic matching," *Computer Vision, Graphics, and Image Processing*, vol. 46, no. 1, pp. 1–21, 1989.
- [14] X. Yang, Y. Li, D. Reutens, and T. Jiang, "Diffeomorphic metric landmark mapping using stationary velocity field parameterization," *International Journal of Computer Vision*, vol. 115, no. 2, pp. 69–86, 2015.
- [15] F.-X. Vialard, L. Risser, D. Rueckert, and C. J. Cotter, "Diffeomorphic 3d image registration via geodesic shooting using an efficient adjoint calculation," *International Journal of Computer Vision*, vol. 97, no. 2, pp. 229–241, 2012.
- [16] A. Pai, S. Sommer, L. Sørensen, S. Darkner, J. Sporring, and M. Nielsen, "Kernel bundle diffeomorphic image registration using stationary velocity fields and wendland basis functions," *IEEE Transactions on Medical Imaging*, vol. 35, no. 6, pp. 1369–1380, 2016.
- [17] X. Yang, R. Kwitt, M. Styner, and M. Niethammer, "Quicksilver: Fast predictive image registration - A deep learning approach," *NeuroImage*, vol. 158, pp. 378–396, 2017.
- [18] A. Dosovitskiy, P. Fischer, E. Ilg, P. Hausser, C. Hazirbas, V. Golkov, P. Van Der Smagt, D. Cremers, and T. Brox, "Flownet: Learning optical flow with convolutional networks," in *IEEE International Conference on Computer Vision*, 2015, pp. 2758–2766.
- [19] E. Ilg, N. Mayer, T. Saikia, M. Keuper, A. Dosovitskiy, and T. Brox, "Flownet 2.0: Evolution of optical flow estimation with deep networks," in *IEEE Conference on Computer Vision and Pattern Recognition*, 2017, pp. 1647–1655.
- [20] Z. Shen, X. Han, Z. Xu, and M. Niethammer, "Networks for joint affine and non-parametric image registration," in *IEEE Conference on Computer Vision and Pattern Recognition*, 2019, pp. 4224–4233.
- [21] X. Hu, M. Kang, W. Huang, M. R. Scott, R. Wiest, and M. Reyes, "Dual-stream pyramid registration network," in *International Conference on Medical Image Computing and Computer Assisted Intervention*, 2019, pp. 382–390.
- [22] S. Zhao, Y. Dong, E. I. Chang, and Y. Xu, "Recursive cascaded networks for unsupervised medical image registration," in *International Conference on Computer Vision*, 2019, pp. 10599–10609.
- [23] A. Hering, B. van Ginneken, and S. Heldmann, "mlvnrnet: Multilevel variational image registration network," in *International Conference on Medical Image Computing and Computer Assisted Intervention*, 2019, pp. 257–265.
- [24] M. Niethammer, R. Kwitt, and F.-X. Vialard, "Metric learning for image registration," in *IEEE Conference on Computer Vision and Pattern Recognition*, 2019, pp. 8463–8472.
- [25] R. Liu, Y. Zhang, S. Cheng, X. Fan, and Z. Luo, "A theoretically guaranteed deep optimization framework for robust compressive sensing mri," in *Proceedings of the AAAI Conference on Artificial Intelligence*, vol. 33, 2019, pp. 4368–4375.
- [26] M. Jaderberg, K. Simonyan, A. Zisserman *et al.*, "Spatial transformer networks," in *Advances in neural information processing systems*, 2015, pp. 2017–2025.
- [27] S. G. Mueller, M. W. Weiner, L. J. Thal, R. C. Petersen, C. R. Jack, W. Jagust, J. Q. Trojanowski, A. W. Toga, and L. Beckett, "Ways toward an early diagnosis in Alzheimer's disease: The Alzheimer's disease neuroimaging initiative (adni)," *Alzheimer's Dementia*, vol. 1, no. 1, pp. 55–66, 2005.
- [28] A. Di Martino, C.-G. Yan, Q. Li, E. Denio, F. X. Castellanos, K. Alaerts, J. S. Anderson, M. Assaf, S. Y. Bookheimer, M. Dapretto *et al.*, "The Autism brain imaging data exchange: towards a large-scale evaluation of the intrinsic brain architecture in Autism," *Molecular psychiatry*, vol. 19, no. 6, pp. 659–667, 2014.
- [29] K. Marek, D. Jennings, S. Lasch, A. Siderowf, C. Tanner, T. Simuni, C. Coffey, K. Kieburz, E. Flagg, S. Chowdhury *et al.*, "The parkinson progression marker initiative (ppmi)," *Progress in Neurobiology*, vol. 95, no. 4, pp. 629–635, 2011.
- [30] D. S. Marcus, A. F. Fotenos, J. G. Csernansky, J. C. Morris, and R. L. Buckner, "Open access series of imaging studies: Longitudinal MRI data in nondemented and demented older adults," *Journal of Cognitive Neuroscience*, vol. 22, no. 12, pp. 2677–2684, 2010.
- [31] D. C. V. Essen, S. M. Smith, D. M. Barch, T. E. J. Behrens, E. Yacoub, and K. Ugurbil, "The WU-Minn human connectome project: An overview," *NeuroImage*, vol. 80, pp. 62–79, 2013.
- [32] B. Fischl, "Freesurfer," *NeuroImage*, vol. 62, no. 2, pp. 774–781, 2012.
- [33] M. W. Woolrich, S. Jbabdi, B. Patenaude, M. Chappell, S. Makni, T. Behrens, C. Beckmann, M. Jenkinson, and S. M. Smith, "Bayesian analysis of neuroimaging data in FSL," *NeuroImage*, vol. 45, no. 1, pp. S173–S186, 2009.
- [34] M. Abadi, A. Agarwal, P. Barham, E. Brevdo, Z. Chen, C. Citro, G. S. Corrado, A. Davis, J. Dean, M. Devin *et al.*, "Tensorflow: Large-scale machine learning on heterogeneous distributed systems," *CoRR*, vol. abs/1603.04467, 2016.
- [35] D. P. Kingma and J. Ba, "ADAM: A method for stochastic optimization," in *International Conference on Learning Representations*, 2015.
- [36] L. Dice, "Measures of the amount of ecologic association between species," *Ecology*, vol. 26, no. 3, pp. 297–302, 1945.

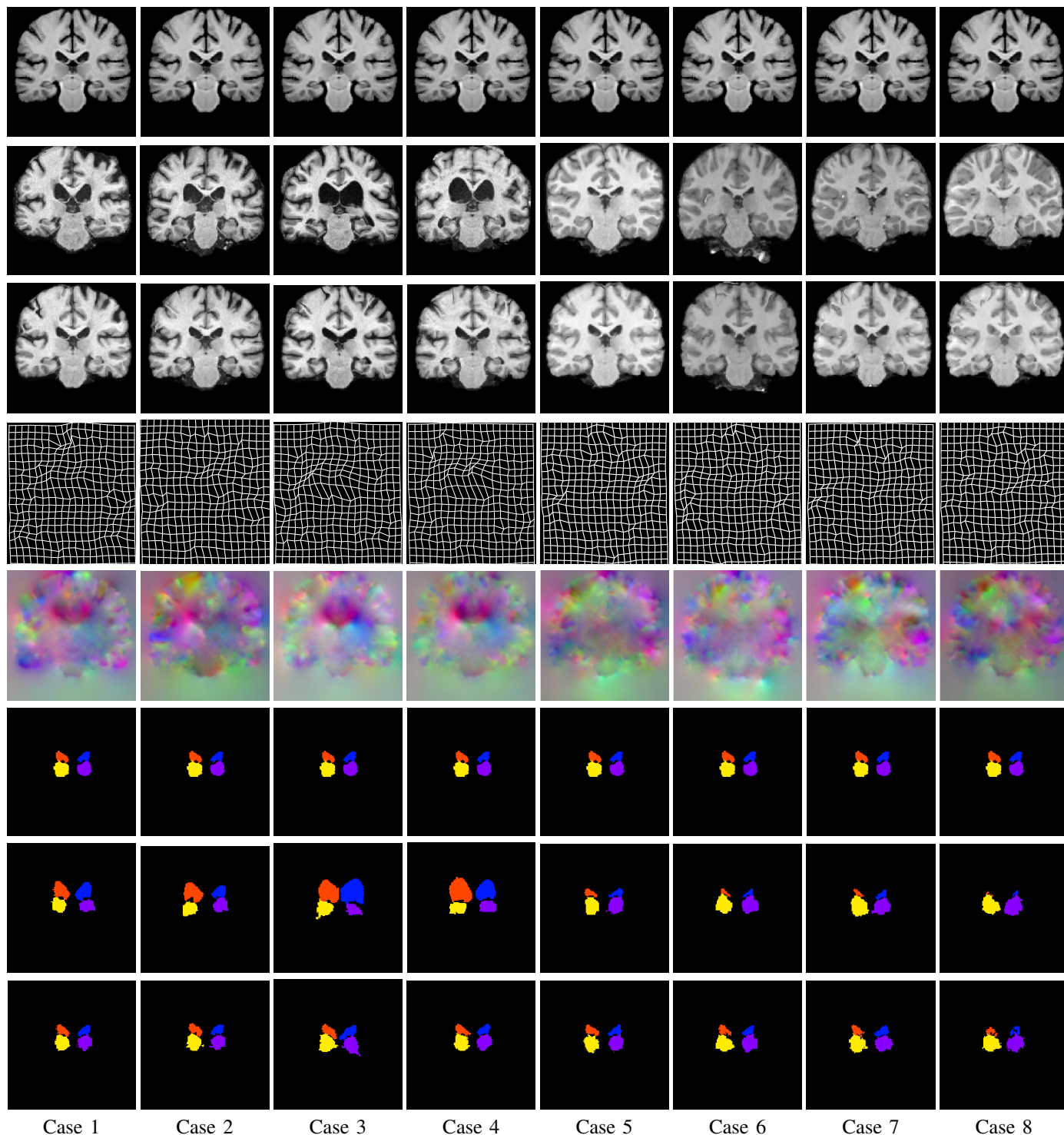


Fig. 10. Eight example registration cases with Case 1-4 from adult data and Case 5-8 from HCP child data. The first five rows refer to target, source, registered images and deformation fields, respectively with the last three rows showing the corresponding label images. The large deformations that exist in the adult scans make registration challenging. For child MR images, due to still in inherent myelination and maturation process, white matter and gray matter exhibit obvious differences in contrast to the fixed image, also making registration difficult. As a result, all the source images are well aligned to the target images and the deformation fields are smooth, demonstrating the excellent registration performance of our approach.

- [37] S. Klein, M. Staring, K. Murphy, M. A. Viergever, and J. P. Pluim, "elastix: A toolbox for intensity-based medical image registration," *IEEE Transactions on Medical Imaging*, vol. 29, no. 1, pp. 196–205, 2010.
- [38] B. B. Avants, C. L. Epstein, M. Grossman, and J. C. Gee, "Symmetric diffeomorphic image registration with cross-correlation: evaluating automated eling of elderly and neurodegenerative brain," *Medical Image Analysis*, vol. 12, no. 1, pp. 26–41, 2008.
- [39] B. B. Avants, N. J. Tustison, G. Song, P. A. Cook, A. Klein, and J. C. Gee, "A reproducible evaluation of ants similarity metric performance in brain image registration," *NeuroImage*, vol. 54, no. 3, pp. 2033–2044, 2011.